Cell Proliferation

Cell Prolif., 2015, **48**, 198–208 doi: 10.1111/cpr.12163

Zinc oxide nanoparticles inhibit murine photoreceptor-derived cell proliferation and migration *via* reducing TGF-β and MMP-9 expression *in vitro*

Da Dong Guo*, Qing Ning Li†, Chun Min Li‡ and Hong Sheng Bi*

**Shandong Provincial Key Laboratory of Integrated Traditional Chinese and Western Medicine for Prevention and Therapy of Ocular Diseases, Key Laboratory of Integrated Traditional Chinese and Western Medicine for Prevention and Therapy of Ocular Diseases in Universities of Shandong, Eye Institute of Shandong University of Traditional Chinese Medicine, Jinan 250002, China, †Zhejiang Provincial Key Laboratory of Pathophysiology, Department of Medicine, School of Medicine, Ningbo University, Ningbo 315211, China and ‡Department of Pharmacy, Jinan Maternity and Child Care Hospital, Jinan 250001, China*

Received 24 August 2014; revision accepted 1 October 2014

Abstract

Objectives: To investigate behaviour and expression of transforming growth factor-β (TGF-β) and matrix metalloproteinases (MMP-9) in murine photoreceptor-derived cells (661W) after incubation with zinc oxide (ZnO) nanoparticles.

Materials and methods: We explored effects of ZnO nanoparticles on 661W cells using a real-time cell electronic sensing system, flow cytometry, multiple function microplate reading, real-time quantitative PCR detection system and enzyme-linked immunosorbent assay respectively.

Results: Our results indicate that ZnO nanoparticles induced overload of calcium and reactive oxygen species within cells, causing formation of apoptotic bodies, disruption of cell cycle distribution, and reduction in expression of TGF-β and MMP-9, to suppress cell proliferation and migration. Our findings show that disruption of intracellular calcium homoeostasis and overproduction of reactive oxygen species were closely associated with reduction of TGF-β and MMP-9 in 661W cells under ZnO nanoparticle treatment.

Conclusions: Results of our study indicate that ZnO nanoparticles suppressed cell proliferation and migration, and reduced production of TGF-β and MMP-9 at both gene and protein levels. Our findings contribute to the understanding of the molecular mechanisms that reduced TGF-β and MMP-9 levels inhibit cell proliferation and migration under ZnO nanoparticle influence.

Correspondence: Hong Sheng Bi, Eye Institute of Shandong University of Traditional Chinese Medicine, Jinan 250002, China. Tel./fax: +8653182861167; E-mail: azuresky1999@163.com

Introduction

Retinal degenerative diseases such as retinitis pigmentosa and age-related macular degeneration, concern loss of photoreceptor cells causing visual loss and possibly eventual blindness. Types of retinal degeneration are progressive disorders initiated by photoreceptor stress and can be accelerated by photoreceptor death (1). Up to now, photoreceptor cell death has usually been regarded to be the common pathway for degeneration of retinal receptors, induced by a variety of factors (for example, heredity or light) (2,3). However, precise causes have remained unclear.

Photoreceptor cell death involves multiple signalling pathways. It has been reported that cytochrome *P450 2C* genes play a direct causative role in their photochemical stress-induced death (4); meanwhile, receptor interacting protein kinase-mediated necrosis and tumour necrosis factor-induced cell necrosis strongly contribute to photoreceptor degeneration in interphotoreceptor retinoid-binding protein (−/−) mice (5). Furthermore, the caspase-independent pathway (6), tumour necrosis factor-α signalling pathway, receptor interacting protein kinase pathway (7) and Fas ligand–Fas signalling pathway (8) have also been shown to be involved in photoreceptor cell death under different stress conditions. Nevertheless, the detailed mechanisms still need to be addressed.

Cell proliferation results in an increment in cell number as a result of cell population growth, cell division, and cell migration being fundamental to organization and maintenance of tissue integrity. Thus, both cell proliferation and migration play crucial roles in

embryonic development, wound healing, inflammation and invasiveness through the extracellular matrix (9), and cell migration critically depends on calcium ion (Ca^{2+}) channel-mediated Ca^{2+} influx (10). As a fundamental secondary intracellular signalling molecule, Ca^{2+} regulates essential cellular functions in various cell types *via* Ca^{2+}-dependent signalling pathways. However, overload of intracellular calcium ions causes intracellular calcium dysfunction and increase in oxidative stress (11–13), which further mediate a variety of physiological and pathological functions. Reactive oxygen species (ROS) are produced as by-products of cell metabolism; they are mainly generated in mitochondria. Normally, ROS levels remain at low levels within cells. Nevertheless, when cell production of ROS overwhelms its antioxidant capacity, they damage cell macromolecules such as lipids, proteins and DNA (14). Moreover, ROS can also modulate various biological functions through stimulating transduction signals (15), including cell apoptosis (16) and cell migration (17,18). Nevertheless, relationships between changes in intracellular [Ca^{2+}] and ROS, migration and proliferation are not yet clear.

Transforming growth factor-β (TGF-β) plays an important role in many cell processes, including adhesion, proliferation, migration, differentiation and cell cycle arrest (19). TGF-β is a multifunctional growth factor that can either stimulate or inhibit cell proliferation, mainly depending on cell type and culture conditions (20). Matrix metalloproteinases (MMPs) compose a large family of calcium-dependent and zinc-containing endopeptidases. They play a crucial role in turnover of extracellular matrix, and function in physiological and pathological processes involved in tissue remodelling. This includes degradation of the extracellular matrix, including collagens, elastins, gelatin, matrix glycoproteins and proteoglycan (21,22). Matrix metalloproteinase-9 (MMP-9), a major component of the basement membrane, is a key enzyme associated with degradation of type IV collagen. MMP-9 can cleave many different targets (for example, extracellular matrix, cytokines, growth factors, chemokines and cytokine/growth factor receptors) that in turn regulate key signalling pathways in cell growth, migration, invasion, inflammation and angiogenesis (23,24). Thus, both TGF-β and MMP-9 are closely associated with cell proliferation and migration in physiological and pathological processes.

Nanoparticles are a type of microscopic particle with at least one dimension less than 100 nm. Due to their unique physical and chemical properties (surface effect and small scale effect), nanoparticles have been widely applied in construction of piezoelectric devices, synthesis of pigments, chemical sensors and more. Zinc oxide (ZnO) nanoparticles have also received much attention due to their biological applications, pharmaceutical and biomedical potentials. It has been reported that ZnO nanoparticles have anti-diabetes benefits (25), anti-bacterial effects (26) and anti-cancer roles (27,28). Meanwhile, analysis of cytotoxic consequences indicate that ZnO nanoparticles can also damage normal cells, such as macrophages (29), retinal ganglion cells (30) and lens epithelial cells (31). These types of damage are involved in phosphatidylinositol 3-kinase (PI3K)-mediated mitogen-activated protein kinase (MAPK) pathway, bcl-2, caspase-9 and caspase-12 signalling as well as calcium-dependent signalling pathways. Considering the biomedical applications of ZnO nanoparticles and their potential hazard to organisms, in the present study, we investigated effects of ZnO nanoparticles on photoreceptor cells.

As a parenchymal cell, photoreceptors are very susceptible to alterations in the external microenvironment. To explore whether ZnO nanoparticles influence intracellular calcium and ROS, TGF-β and MMP-9 and consequences to photoreceptor cell migration and proliferation, in this study, we used 661W cells, a murine photoreceptor-derived cell line transformed by SV40, to investigate effects of various concentrations of ZnO nanoparticles on cell proliferation and migration. We also assessed underlying alterations in intracellular Ca^{2+}, ROS, cell nuclei and cell cycle distribution after treatment with various concentrations of ZnO nanoparticles. We report here that ZnO nanoparticles inhibited murine photoreceptor-derived cell proliferation and migration *via* reducing TGF-β and MMP-9 expression.

Materials and methods

Characterization of ZnO nanoparticles

Zinc oxide nanoparticles (ZP6) capped with aminopolysiloxane were characterized using transmission electron microscopy (HT7700; Hitachi, Tokyo, Japan).

Preparation of ZnO nanoparticle stock solution

Zinc oxide nanoparticles were dispersed in Dulbecco's modified Eagle's medium (DMEM; Life Technologies, Gaithersburg, MD, USA) containing 1.0 g/l glucose, 10% foetal bovine serum (HyClone, Logan, UT, USA), and final concentration of ZnO nanoparticle stock solution was 1.0 mg/mL. Prior to experimentation, stock solution was sonicated in a water-ice bath using an ultrasonic cell crusher (Bilon92-IIDL, Xian, China) at 30 kHz for 20 min, to obtain a uniform colloidal suspension, then diluted with DMEM to the indicated concentrations.

Cell culture

Murine photoreceptor-derived cell line 661W, was kindly provided by Dr. Muayyad R. Al-Ubaidi (University of Oklahoma Health Sciences Center, USA). 661W cells were maintained in DMEM supplemented with 10% foetal bovine serum (HyClone), 1.0 g/l glucose, 100 U/ml penicillin and 100 μg/ml streptomycin. All cells were cultured at 37 °C in a water-saturated air incubator with 5% CO_2 and cell counting was performed using an automated cell counter (TC10; Bio-Rad, Hercules, CA, USA).

In vitro *cell proliferation*

To explore effects of different concentrations of ZnO nanoparticles on 661W cell proliferation *in vitro*, real-time cell electronic sensing (RT-CES) assay was performed. RT-CES technology provides dynamic information concerning the target cells after treatment with chemicals, which allows for their non-invasive monitoring by means of impedance sensor technology. RT-CES is also a valuable, sensitive and reliable technology, which can monitor the cellular events by determining changes of electrical impedance between micro-electrodes integrated into the bottom of custom made tissue culture plates (E-plates) (32,33), in real-time. In this study, RT-CES (ACEA Biosciences Inc., Hangzhou, China) was used to determine interactions between 661W cells and different concentrations of ZnO nanoparticles. In brief, 6000 cells were seeded into each well of the E-plate and cultured overnight. Then they were treated with a range of concentrations (0, 2.5, 5.0 and 10.0 μg/ml) of ZnO nanoparticles and further cultured for an additional 72 h. Data on cell proliferation after treatment with ZnO nanoparticles were expressed as normalized cell index.

In vitro *cell migration*

To investigate migratory effects of different concentrations of ZnO nanoparticles on 661W cell migration *in vitro*, first, the cells were pre-treated with the concentrations (0, 2.5, 5.0 and 10.0 μg/ml) of ZnO nanoparticles at 37 °C for 1 h (1.0×10^4 cells per well) and resuspended in serum-free DMEM and placed in the upper chamber of CIM-Plate 16 (ACEA Biosciences (Hangzhou) Inc., China). As chemoattractant, the lower chamber contained 165 μl total ingredient medium (containing 10% foetal bovine serum). In contrast, untreated cells were also seeded in serum-free DMEM in both lower and upper chambers, as a negative control. Subsequently, data acquisition was initiated immediately and was maintained at 37 °C for 14 h when both lower chamber and upper chamber were completely assembled on the RT-CES analyser.

Real-time analysis of intracellular $[Ca^{2+}]$

After treatment with various concentrations of ZnO nanoparticles, real-time measurement of intracellular $[Ca^{2+}]$ was performed using Fluo-4 indicator (Invitrogen, Carlsbad, CA, USA). Briefly, 661W cells (1.0×10^4 per well) were seeded in a black-walled 96-well plate (Costar, Cambridge, MA, USA) at 37 °C in a water-saturated 5% CO_2 incubator overnight, then culture medium was replaced with 150 μl Fluo-4/AM solution (Invitrogen) and incubated for 30 min in the presence of DMEM. After washing twice in DMEM, the concentrations (0, 2.5, 5.0 and 10.0 μg/ml) of ZnO nanoparticle solution were added to each well, and real-time responses of intracellular $[Ca^{2+}]$ were recorded immediately at 37 °C using a Multiple Function Microplate Reader (EnSpire & Dispenser; PerkinElmer, Norwalk, CT, USA) with excitation wavelength of 495 nm and emission wavelength of 515 nm.

Measurement of intracellular ROS

Effects of ZnO nanoparticles on intracellular ROS levels were measured with 2′, 7′-dichlorofluorescin diacetate (DCFH-DA; Invitrogen) by flow cytometry (Accuri C6, Ann Arbor, MI, USA). Briefly, 661W cells (3×10^5 cells per well) were seeded in a 6-well plate (final volume: 2 ml, NEST Biotechnology, Wuxi, China) and grown overnight; supernatant was then discarded and cells were supplemented with 0, 2.5, 5.0 and 10.0 μg/ml of ZnO nanoparticle solution. After incubation for 2 h, cells were washed in phosphate buffered saline (PBS, pH 7.4) twice, incubated in DCFH-DA solution (10 μM) in constant darkness at 37 °C for 30 min, washed twice in PBS and measured by flow cytometry within 30 min. Specific fluorescence signals corresponding to DCFH-DA were collected using a 525-nm band pass filter. As a rule, 1.0×10^4 cells were analysed for each determination. Experiments were repeated three times and results are expressed as mean ± SD.

DAPI staining

To explore effects of ZnO nanoparticles on 661W cell nuclei, DAPI nuclear staining was performed after cells had been treated with the appropriate concentrations of ZnO nanoparticles, for 24 h. Briefly, 661W cells (6×10^4 cells per well) were seeded in a 6-well plate

(NEST Biotechnology) and grown overnight, then incubated with different concentrations (0, 2.5, 5.0 and 10.0 μg/ml) of ZnO nanoparticles (final volume: 2 ml) for 24 h. Cells were washed in PBS at indicated time points and fixed in 4% polymerisatum for 15 min. After fixation, cells were washed twice in PBS and subsequently stained with 1 μg/ml DAPI staining solution (Pierce Biotechnology, Rockford, IL, USA) for 30 min. Finally, all stained cells were examined using an inverted fluorescence microscope (Olympus IX71, Tokyo, Japan).

Analysis of cell cycle distribution

To investigate effects of ZnO nanoparticles on cell cycle distribution, cell cycle analysis was performed using flow cytometry. In brief, 661W cells (4×10^5 cells per well) were seeded in a 6-well plate and cultured at 37 °C overnight, then treated with different concentrations (0, 2.5, 5.0 and 10.0 μg/ml respectively) of ZnO nanoparticles and cultured for an additional 24 h. After harvesting with 0.25% trypsin, all cells were washed twice in ice-cold PBS, resuspended in ice-cold 70% ethanol and kept at 4 °C overnight. Further, cells were washed twice in ice-cold PBS and co-incubated with 50 mg/l propidium iodide (PI) (Beyotime, Nantong, China) and RNase (60 μg/ml) in constant darkness at 37 °C for 40 min. Finally, cell cycle distribution of each sample was determined by flow cytometry (Accuri C6).

Gene expression analysis of TGF-β and MMP-9

To investigate alterations in TGF-β and MMP-9 mRNA, 661W cells were treated with the different concentrations (0, 2.5, 5.0 and 10 μg/ml) of ZnO nanoparticles and cultured in a CO_2 incubator at 37 °C for 2 h. At the indicated time point, total RNA was isolated using TRIzol reagent (Invitrogen) according to the manufacturer's instructions, and was quantified using a K5600 spectrophotometer (Beijing Kaiao Technology Development Co., Ltd., Beijing, China) before reverse transcription using RevertAid reverse transcriptase kit (Fermentas, Burlington, ON, Canada). Real-time quantitative PCR was performed using SYBR Green Master Mix (Aidlab, Beijing, China) and Stratagene Mx3000P sequence detection system (Agilent Technologies, Palo Alto, CA, USA). Primers were designed by Premier 5.0 software and were synthesized by Shanghai Sangon Biological Engineering Technology and Service Company (Shanghai, China). Primers for TGF-β were 5′-tgagtggctgtcttttgacg-3′ (forward) and 5′-tggggctgatcccgttgatt-3′ (reverse). Primers for MMP-9 were 5′-ggatgtttttgatgctattgctg-3′ (forward) and 5′-acgtgcgggcagtaaggaag-3′ (reverse), and primers for GAPDH were 5′-gaccacagtccatgccatcact-3′ (forward) and 5′-tccaccaccctgttgctgtag-3′ (reverse) respectively. The PCR program was set as follows: 95 °C for 5 min, followed by 45 cycles of a 95 °C denaturation for 20 s, 56 °C annealing for 20 s and 72 °C extension for 20 s. Each experiment was performed in triplicate and was repeated three times. ΔΔct values were calculated as fold change in expression over 661W cells in CM ± SEM after normalization to respective endogenous GAPDH control.

Determination of intracellular TGF-*β and MMP-9 proteins*

After treatment with the different concentrations of ZnO nanoparticles, amounts of intracellular TGF-β and MMP-9 protein in the cells were determined by ELISA. The murine TGF-β ELISA kit was purchased from Dakewe Biotech Co. Ltd (Beijing, China) and murine MMP-9 ELISA kit was purchased from Wuhan ColorfulGene Biological Technology Co., Ltd. (Wuhan, China) respectively. Briefly, 661W cells were seeded in a 6-well plate at a density of 3×10^5 cells/well and grown overnight; medium was then discarded and replaced with different concentrations (0, 2.5, 5.0 and 10.0 μg/ml respectively) of ZnO nanoparticles (final volume: 2 ml). After exposing the cells to ZnO nanoparticles for 5 h, they were digested with 0.25% trypsin and were collected by centrifugation at 3000 ***g*** for 10 min. Subsequently, cell pellets were rinsed in cold PBS and centrifuged to collect the cells. Further, cells were resuspended in 0.5 ml of cold PBS and sonicated in an ice bath for 10 min. After centrifugation at 5000 ***g*** for 10 min, level of either TGF-β or MMP-9 protein from cell extract in 100 μl of supernatant was measured by ELISA, according to the manufacturer's instructions. All samples were measured in triplicate and repeated three times.

Statistical analysis

Every experiment was repeated three times and all results are presented as mean ± SD. For statistical analysis, Student's *t*-test and ANOVA followed by Dunn's *post hoc* tests were performed. P value <0.05 was considered to be statistically significant.

Results

Characterization of ZnO nanoparticles

Average diameter of ZnO nanoparticles measured using transmission electron microscopy was in the order of

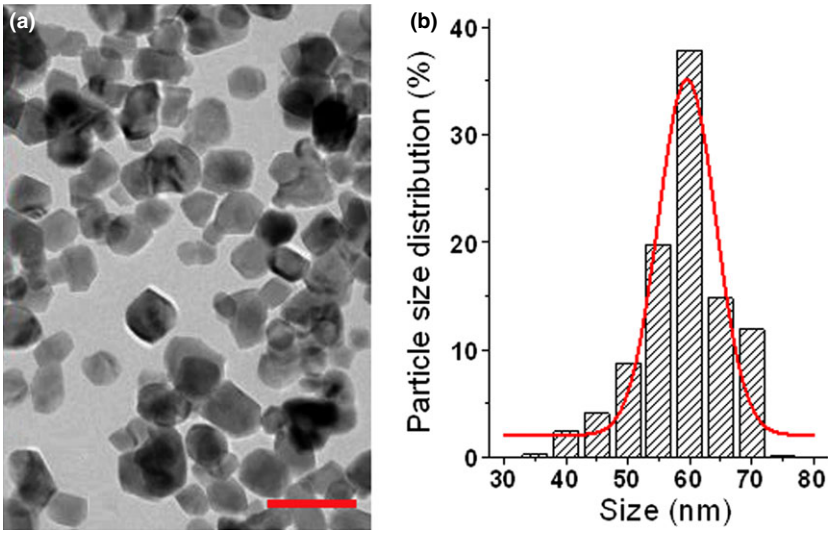

Figure 1. Zinc oxide nanoparticles captured by transmission electron microscopy (a) and statistical analysis of zinc oxide nanoparticle size distribution (b). Bar indicates 100 nm.

60 nm (Fig. 1a); histogram of ZnO nanoparticle size distribution is shown in Fig. 1b.

RT-CES assay

Compared to traditional end-point assays, the RT-CES system has the benefit of non-invasion, by recording values of impedance, which can continuously and quantitatively record dynamic processes of cytotoxic activity. Here, we used RT-CES assay to assess effects of different concentrations of ZnO nanoparticles on 661W cell proliferation. As shown in Fig. 2a, 2.5 μg/ml ZnO nanoparticles produced a cytotoxic effect on 661W cells, that is, ZnO nanoparticles suppressed 661W cell proliferation. Meanwhile, we observed that with increase in ZnO nanoparticles there was a markedly inhibitory effect of them on the cells, which was dose-dependent. Moreover, results of statistical analysis at 24, 48 and 72 h (Fig. 2b) were in agreement with determination of MTT assay (data not shown).

Cell migration analysis

The capacity of ZnO nanoparticles to inhibit cell migration was also investigated using the RT-CES system. As shown in Fig. 3, the capacity of cell migration was reduced after treatment with ZnO nanoparticles compared to untreated cells (lower chamber containing DMEM with foetal bovine serum) (Fig. 3a), and was concentration-dependent (Fig. 3b–d). However, capacity of migration was the poorest for cells treated with serum-free DMEM in both upper and lower chambers (Fig. 3e).

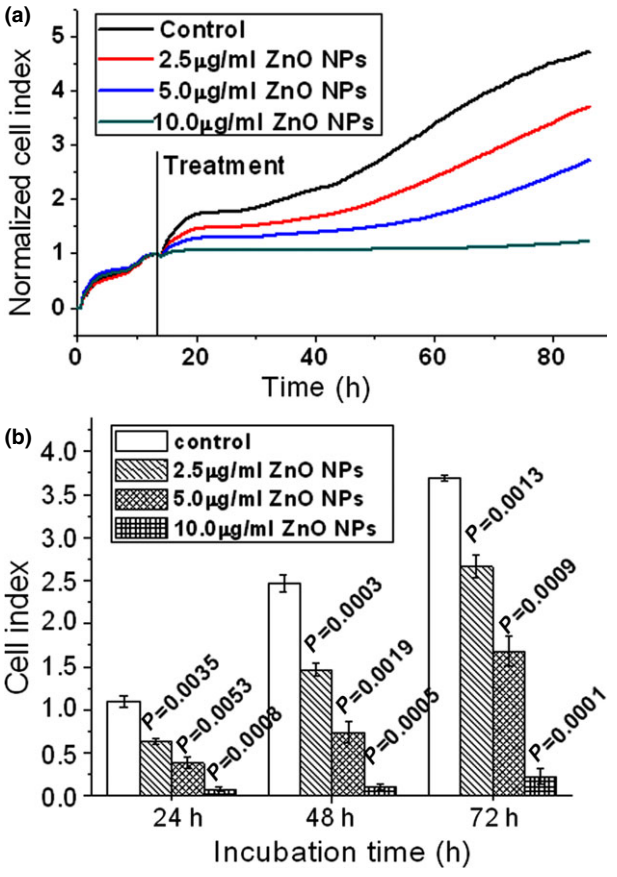

Figure 2. Dynamic responses of murine photoreceptor-derived cells after exposure to designated concentrations of ZnO NPs. (a) Cells were treated with appropriate concentrations of ZnO NPs for 72 h; (b) statistical results compared to relevant controls after treatment with designated concentrations of ZnO NPs for 24, 48 and 72 h respectively. ZnO, zinc oxide; NPs, nanoparticles.

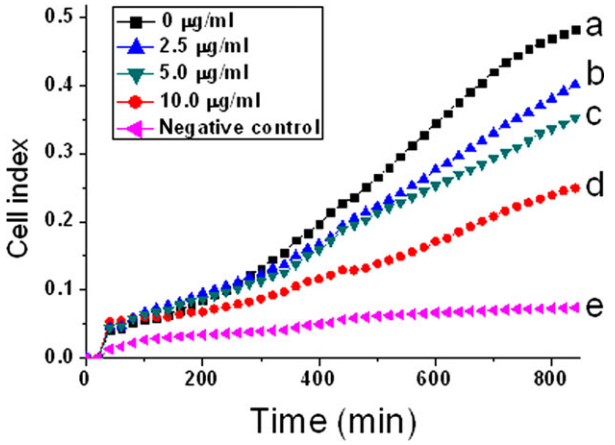

Figure 3. Zinc oxide nanoparticles suppressed 661W cell migration. Real-time measurements of cell impedance performed using a real-time cell electronic sensing system. Cells were pre-treated with ZnO nanoparticles for 1 h, and were then resuspended in serum-free medium and placed in the upper chamber of CIM-Plate 16. Meanwhile, the lower chambers contained 165 μl of DMEM medium supplemented with 10% foetal bovine serum (a–d). By contrast, cells seeded in serum-free DMEM in both lower and upper chambers were as negative control (e).

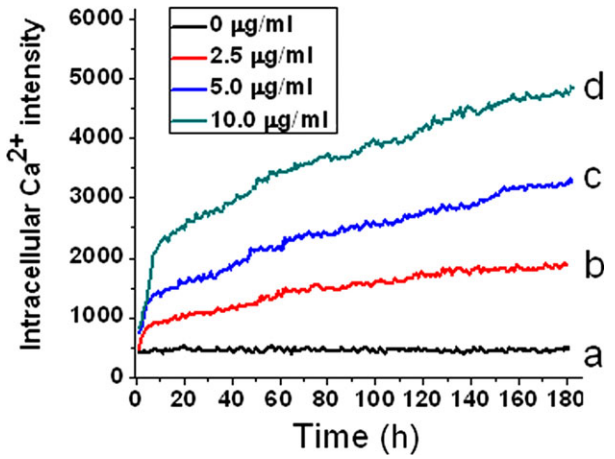

Figure 4. Dynamic fluorescence measurements of intracellular [Ca^{2+}] in murine photoreceptor-derived cells after treatment with designated concentrations of zinc oxide nanoparticles. Cells were seeded in a 96-well plate and grown overnight; they were then loaded with Fluo-4 probe. After washing twice in DMEM, appropriate concentrations of zinc oxide nanoparticles were separately added in each well automatically, and data were determined immediately by a Multiple Function Microplate Reader.

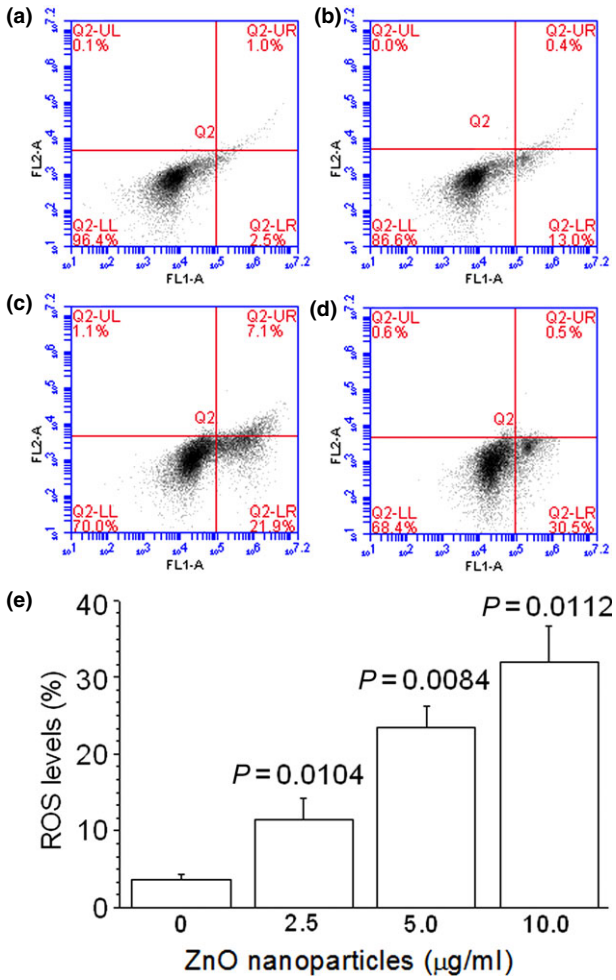

Figure 5. Elevated reactive oxygen species levels of murine photoreceptor-derived cells determined by flow cytometry after exposure to designated concentrations of ZnO NPs for 2 h. (a) Untreated cells; (b) cells treated with 2.5 μg/ml of ZnO NPs; (c) cells treated with 5.0 μg/ml of ZnO NPs; (d) cells treated with 10.0 μg/ml of ZnO NPs and (e) statistical result of three independent experiments. ZnO, zinc oxide; NPs, nanoparticles.

Dynamic [Ca^{2+}] determination

Dynamic measurement of [Ca^{2+}] provides real-time responses to various treatments to target cells. As shown in Fig. 4, kinetic fluorescence measurements of 661W cells indicated that after exposing them to elevated concentrations of ZnO nanoparticles, intracellular [Ca^{2+}] was also higher, and was concentration-dependent (Fig. 4b–d). However, intracellular [Ca^{2+}] in 661W cells alone (cells cultured with DMEM only) remained at a constant stable level (Fig. 4a).

Measurement of intracellular ROS

After the cells were exposed to the various concentrations of ZnO nanoparticles for 2 h, intracellular ROS levels were elevationed (Fig. 5a–d). Intracellular ROS levels rose from 2.73 ± 0.59% to 12.07 ± 2.24%,

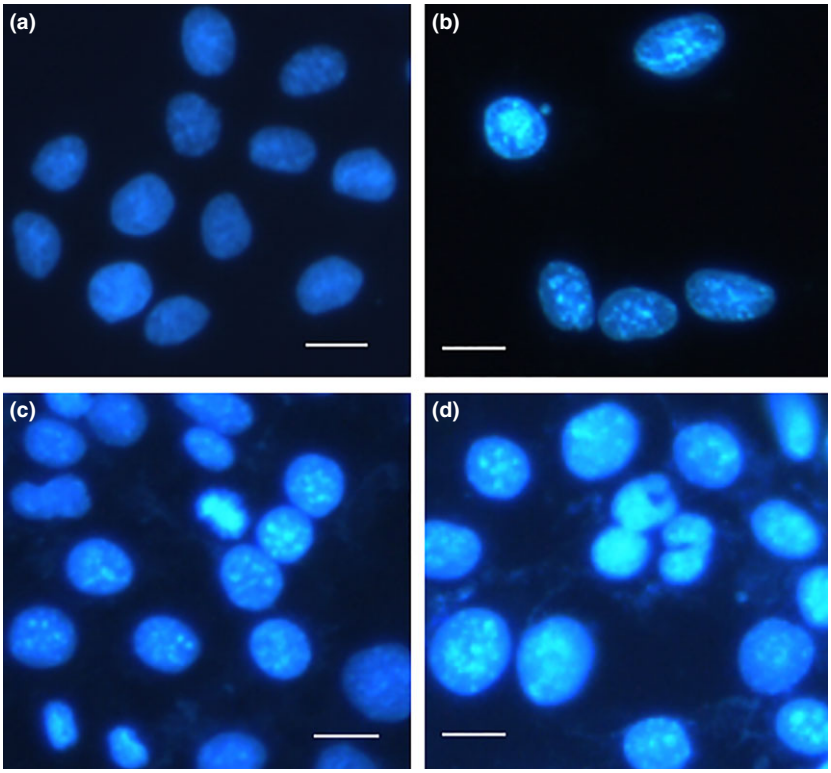

Figure 6. Typical nuclear morphological alterations in 661W cells after treatment with appropriate concentrations of ZnO NPs for 24 h. (a) Untreated cells; (b) cells treated with 2.5 μg/ml ZnO NPs; (c) cells treated with 5.0 μg/ml ZnO NPs and (d) cells treated with 10.0 μg/ml ZnO NPs. Bar = 10 μm and ZnO, zinc oxide; NPs, nanoparticles.

22.20 ± 2.69% and 30.63 ± 5.25% (Fig. 5e) respectively. These findings indicate that with incrementation in concentration of cells exposed to ZnO nanoparticles, intracellular ROS levels were also elevated, in a concentration-dependent manner (Fig. 5e).

DAPI staining

To investigate effects of designated concentrations of ZnO nanoparticles on cell morphology, 661W cells were incubated with the different concentrations of ZnO nanoparticles for 24 h. By fluorescence microscopy we found that nuclei in untreated cells exhibited distinct boundaries and were homogeneous (Fig. 6a), whereas cells exposed to ZnO nanoparticles had apparently concentration-dependent canonical apoptotic changes, including rippled or creased nuclei (Fig. 6b), nuclear condensation (Fig. 6c,d) and apoptotic body production (Fig. 6d). Also, we noted that ZnO nanoparticle-induced cytotoxicity became progressively important with incremental ZnO nanoparticles.

Changes in cell cycle distribution

After treatment with designated concentrations of ZnO nanoparticles, alterations in cell cycle distribution were further explored to assess cytotoxic effects of ZnO nanoparticles on the 661W cells. Figure 7a illustrates that the majority of untreated cells were in the growth phase (G1) of cell population, wherein a wide range of enzymes (especially for DNA replication) are synthesized. However, after treatment with ZnO nanoparticles, ratio of G1 phase cells was reduced (Fig. 7b–d), and the ratio of sub-G1 phase was apparently increased in a dose-dependent manner (Fig. 7e). Meanwhile, G2/G1 ratio was also markedly higher for ZnO nanoparticle-treated cells compared to untreated cells, which was significantly statistically different (Fig. 7f).

Alterations in TGF-β and MMP-9

Zinc oxide nanoparticle-treatment reduced TGF-β and MMP-9 at both mRNA and protein levels in 661W cells. As shown in Fig. 8a, after treatment with the designated concentrations (2.5, 5.0 and 10.0 μg/ml) of ZnO nanoparticles, TGF-β mRNA levels were reduced to 0.487 ± 0.162, 0.270 ± 0.209, 0.128 ± 0.056 respectively, and MMP-9 mRNA levels were reduced to 0.820 ± 0.182, 0.513 ± 0.194, 0.377 ± 0.111 respectively. Regarding TGF-β and MMP-9 protein expression, we noted that levels of TGF-β protein were reduced from 53.46 ± 6.46 pg/ml (untreated cells) to 44.25 ± 4.96, 27.93 ± 4.64, 13.98 ± 3.29 pg/ml respectively; meanwhile, levels of MMP-9 protein were reduced from

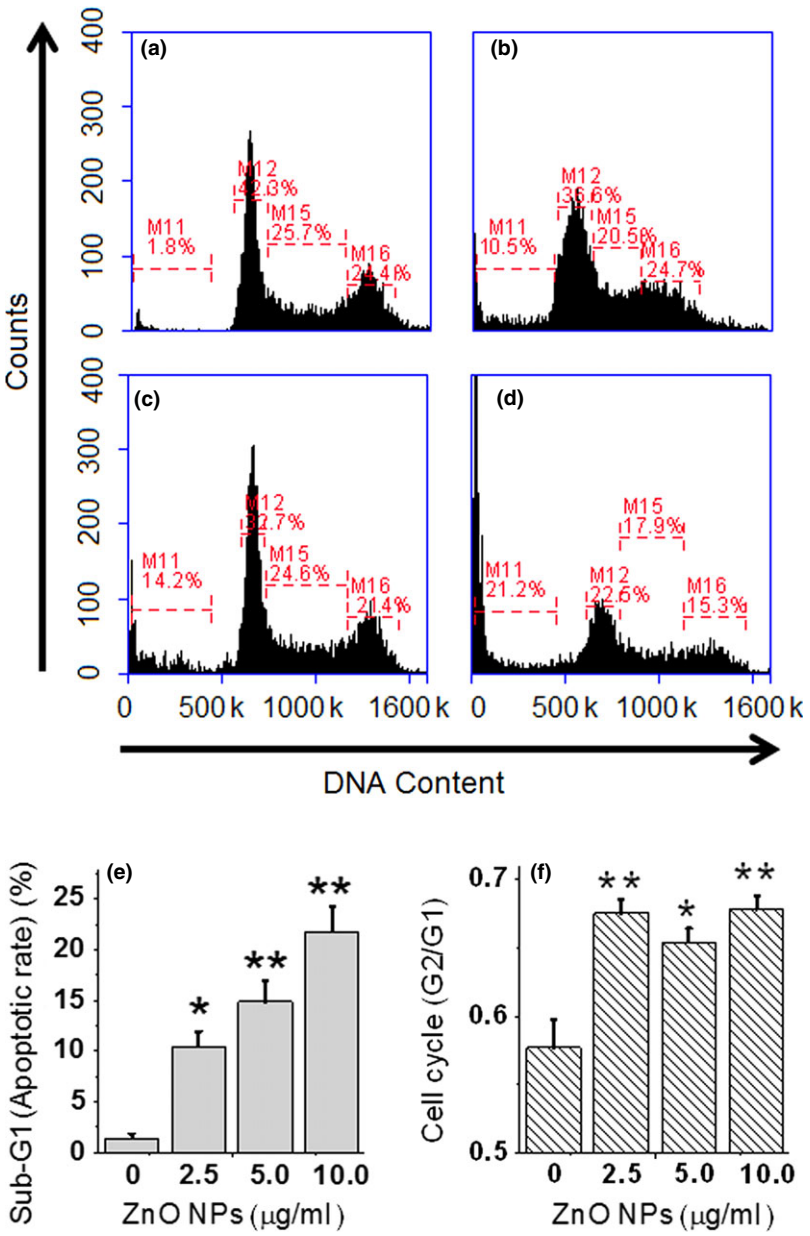

Figure 7. Effects of designated concentrations of ZnO nanoparticles on cell cycle distribution and apoptotic index. Flow cytometric analysis was performed for cell cycle distribution of 661W cells after exposure to (a) 0 μg/ml (control); (b) 2.5 μg/ml; (c) 5.0 μg/ml and (d) 10.0 μg/ml of ZnO nanoparticles for 24 h; (e) quantitative analysis of apoptosis in different treatment groups and (f) alterations in the level of cell cycle distribution. $*P < 0.05$ and $**P < 0.01$ compared to the relevant control group.

92.37 ± 3.30 pg/ml to 82.43 ± 2.68, 75.04 ± 4.07, 64.48 ± 2.70 pg/ml respectively (Fig. 8b).

Discussion

Cell migration is an important factor in the process of precise regulation between cell adhesion and dissociation from extracellular matrix proteins (34). Accordingly, inhibiting migration leads to distinct functional impairment, including influencing wound healing capacity (35). Zhou *et al.* reported that ZnO nanoparticles impeded both cell migration and wound healing progress in both fibroblasts and epithelial cells (36). Also, proliferation and migration are confirmed as being important events involved in the process of photoreceptor cell death (37). In our study, we used different concentrations of ZnO nanoparticles to investigate effects on photoreceptor-derived cell proliferation and migration, and found that exposure to ZnO nanoparticles reduced cell viability in a concentration-dependent manner. Moreover, we also noted that pre-treatment with ZnO nanoparticles for 1 h hardly affected cell viability (that is, there was little cytotoxicity). However, we found that pre-treatment with ZnO nanoparticles efficiently retarded

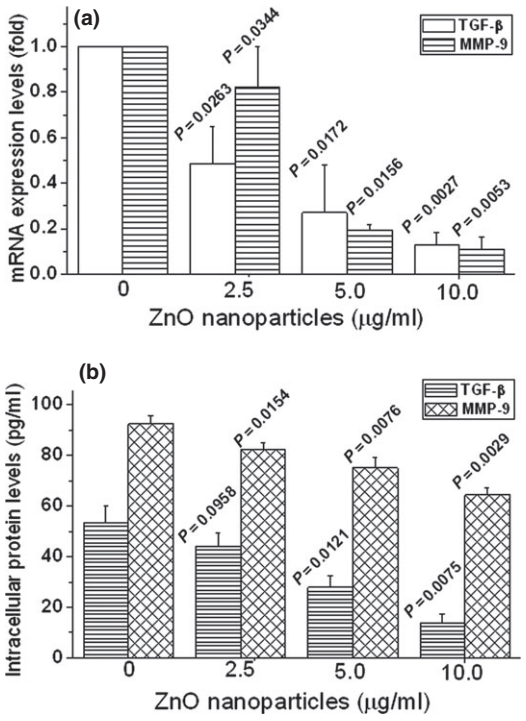

Figure 8. Zinc oxide (ZnO) nanoparticles reduced expression of transforming growth factor-β (TGF-β) and matrix metalloproteinases (MMP-9) in 661W cells. Alterations in TGF-β and MMP-9 both at mRNA (a) and protein (b) levels were performed using quantitative real-time PCR and ELISA respectively. Cells were exposed to designated concentrations of ZnO nanoparticles either for 2 h (for mRNA determination) or for 5 h (for protein determination). Results represented as mean ± SD of three independent experiments.

cell migration in a concentration-dependent manner. Nevertheless, Suzuki *et al.* found that ZnO nanoparticles induce cell migration and adhesion of THP-1 cells (human monocytic leukaemia cells) to HUVECs (human umbilical vein endothelial cells), and accelerate foam cell formation (38). Moreover, Akhtar found that ZnO nanoparticles exerted distinct effects on mammalian cell viability by killing human hepatocellular carcinoma HepG2, human lung adenocarcinoma A549 and human bronchial epithelial BEAS-2B cancer cells, while exerting no influence on normal rat astrocytes and hepatocytes (39). Based on these findings, we infer that ZnO nanoparticle inhibition of cell proliferation and migration is mainly associated with the cell type.

On the one hand, it has been accepted that cell migration critically depends on calcium channel-mediated Ca^{2+} influx, which alters intracellular calcium level and generates [Ca^{2+}] gradients (32,40,41). On the other hand, mitochondria are a major intracellular source of free radicals, and high level of intracellular mitochondrial calcium can enhance free radical generation (42). Thus, elevated intracellular [Ca^{2+}] will disrupt intracellular calcium homoeostasis, causing mitochondrial dysfunction and leading to oxidative stress. Oxidative stress mediates a number of physiological and pathological functions, including cell migration. It has been reported that elevation of intracellular ROS enhances vascular endothelial cell migration (10); meanwhile, ROS can also promote vascular smooth muscle cell proliferation and migration (43). For nanoparticles, due to their small size and large surface area, they are generally thought to induce ROS generation and cellular oxidative stress (44). In our study, we found that exposing photoreceptor cells to ZnO nanoparticles elevated intracellular [Ca^{2+}], disrupted intracellular calcium homoeostasis, and thus caused mitochondrial dysfunction. As a consequence, mitochondrial dysfunction further generates excessive ROS within cells, causing oxidative stress, and finally influences cell migration. It has been reported that low ROS levels are necessary for maintaining normal cell processes, whereas high ROS levels exert deleterious effects on cell functions including cell migration (45,46). In our study, we observed that elevated intracellular ROS inhibited rather than enhanced cell migration. The result that ZnO nanoparticles suppressed photoreceptor cell migration may be owing to the fact that overproduction of ROS impairs normal cell functions and thus inhibits cell migration when exposing photoreceptor cells to ZnO nanoparticles.

Cell cycle progression is partially controlled by balance between accumulation of ROS and the antioxidant system, and disturbance can lead to abnormal cell proliferation during cell division (47). In the present study, a high sub-G1 cell population was found when exposing target cells to ZnO nanoparticles; this result was in agreement with that of exposing human liver cells to nickle nanoparticles (48). In the meantime, we also found that with elevation of ZnO nanoparticles exposure to cells, G2/G1 ratio was also increased, suggesting that alterations of G1, S and G2/M phases were also closely associated with cell proliferation, and were probably involved in the apoptotic pathway.

Both TGF-β and MMP-9 regulate cell growth in different ways (49,50). The central function of TGF-β is to inhibit cell cycle progression by regulating transcription of cell cycle regulators (19). Meanwhile, it also induces MMP-9 expression and cell migration *via* a TGF- β type I receptor (9). In our study, we found that exposing murine photoreceptor-derived cells to ZnO nanoparticles reduced expression of TGF-β and MMP-9 and subsequently reduced capacity of cell proliferation and migration. As a result, the reduced TGF-β and MMP-9 could not efficiently trigger cell proliferation- and migration-related signalling pathways and thereby suppressed target cell proliferation and migration. Our results indicate

the crucial roles of both TGF-β and MMP-9 in regulating cell proliferation and migration.

In conclusion, we have investigated effects of ZnO nanoparticles on murine photoreceptor-derived cells. We found that ZnO nanoparticles efficiently inhibited cell proliferation and migration, induced overload of Ca^{2+} within cells and caused intracellular ROS overproduction, further disrupting normal cell cycle distribution. Moreover, ZnO nanoparticles also reduced TGF-β and MMP-9 expression at both mRNA and protein levels and further impaired cell proliferation and migration. Taken together, our results demonstrate that disruption of intracellular calcium homoeostasis and overproduction of ROS induced by ZnO nanoparticles were mainly responsible for suppressing TGF-β and MMP-9 expression in murine photoreceptor-derived cells. Reduced TGF-β and MMP-9 levels played an important role in suppressing murine photoreceptor-derived cell proliferation and migration in the presence of ZnO nanoparticles.

Acknowledgements

This work was supported by the Development Project of Medicine and Health Science Technology of Shandong Province (2013WS0251), the Development Project of Science and Technology of Traditional Chinese Medicine of Shandong Province (2013ZDZK-083), National Natural Science Foundation of China (no. 81201185) and Innovation Team Project of Ningbo (2011B82014).

Conflict of interest

The authors declare that they have no competing interests.

References

1 Lin Y, Jones BW, Liu A, Vazquéz-Chona FR, Lauritzen JS, Ferrell WD *et al.* (2012) Rapid glutamate receptor 2 trafficking during retinal degeneration. *Mol. Neurodegener.* **7**, 1–14.

2 Sancho-Pelluz J, Arango-Gonzalez B, Kustermann S, Romero FJ, van Veen T, Zrenner E *et al.* (2008) Photoreceptor cell death mechanisms in inherited retinal degeneration. *Mol. Neurobiol.* **38**, 253–269.

3 Cachafeiro M, Bemelmans AP, Samardzija M, Afanasieva T, Pournaras JA, Grimm C *et al.* (2013) Hyperactivation of retina by light in mice leads to photoreceptor cell death mediated by VEGF and retinal pigment epithelium permeability. *Cell Death Dis.* **4**, e781.

4 Chang Q, Berdyshev E, Cao D, Bogaard JD, White JJ, Chen S *et al.* (2014) Cytochrome P450 2C epoxygenases mediate photochemical stress-induced death of photoreceptors. *J. Biol. Chem.* **289**, 8337–8352.

5 Sato K, Li S, Gordon WC, He J, Liou GI, Hill JM *et al.* (2013) Receptor interacting protein kinase-mediated necrosis contributes to cone and rod photoreceptor degeneration in the retina lacking interphotoreceptor retinoid-binding protein. *J. Neurosci.* **33**, 17458–17468.

6 Donovan M, Doonan F, Cotter TG (2006) Decreased expression of pro-apoptotic Bcl-2 family members during retinal development and differential sensitivity to cell death. *Dev. Biol.* **291**, 154–169.

7 Murakami Y, Miller JW, Vavvas DG (2011) RIP kinase-mediated necrosis as an alternative mechanism of photoreceptor death. *Oncotarget* **2**, 497–509.

8 Chang Q, Peter ME, Grassi MA (2012) Fas ligand-Fas signaling participates in light-induced apoptotic death in photoreceptor cells. *Invest. Ophthalmol. Vis. Sci.* **53**, 3703–3716.

9 Hsieh HL, Wang HH, Wu WB, Chu PJ, Yang CM (2010) Transforming growth factor-β1 induces matrix metalloproteinase-9 and cell migration in astrocytes: roles of ROS-dependent ERK- and JNK-NF-κB pathways. *J. Neuroinflamm.* **7**, 88.

10 Sarmiento D, Montorfano I, Cerda O, Cáceres M, Becerra A, Cabello-Verrugio C *et al.* (2014) Increases in reactive oxygen species enhance vascular endothelial cell migration through a mechanism dependent on the transient receptor potential melastatin 4 ion channel. *Microvasc. Res.* 2014 Feb 9. pii: S0026-2862(14)00032-6. doi: 10.1016/j.mvr.2014.02.001. [Epub ahead of print].

11 Capel F, Demaison L, Maskouri F, Diot A, Buffiere C, Mirand PP *et al.* (2005) Calcium overload increases oxidative stress in old rat gastrocnemius muscle. *J. Physiol. Pharmacol.* **56**, 369–380.

12 Yücel D, Aydoğdu S, Cehreli S, Saydam G, Canatan H, Senes M *et al.* (1998) Increased oxidative stress in dilated cardiomyopathic heart failure. *Clin. Chem.* **44**, 148–154.

13 Peng TI, Jou MJ (2010) Oxidative stress caused by mitochondrial calcium overload. *Ann. N. Y. Acad. Sci.* **1201**, 183–188.

14 Thannickal VJ, Fanburg BL (2000) Reactive oxygen species in cell signaling. *Am. J. Physiol. Lung Cell Mol. Physiol.* **279**, L1005–L1028.

15 Bonnefont-Rousselot D (2002) Glucose and reactive oxygen species. *Curr. Opin. Clin. Nutr. Metab. Care* **5**, 561–568.

16 Guo D, Bi H, Liu B, Wu Q, Wang D, Cui Y (2013) Reactive oxygen species-induced cytotoxic effects of zinc oxide nanoparticles in rat retinal ganglion cells. *Toxicol. In Vitro* **27**, 731–738.

17 Bruder-Nascimento T, Chinnasamy P, Riascos-Bernal DF, Cau SB, Callera GE, Touyz RM *et al.* (2014) Angiotensin II induces Fat1 expression/activation and vascular smooth muscle cell migration via Nox1-dependent reactive oxygen species generation. *J. Mol. Cell. Cardiol.* **66**, 18–26.

18 Frijhoff J, Dagnell M, Augsten M, Beltrami E, Giorgio M, Östman A (2014) The mitochondrial reactive oxygen species regulator p66Shc controls PDGF-induced signaling and migration through protein tyrosine phosphatase oxidation. *Free Radic. Biol. Med.* **68**, 268–277.

19 Kubiczkova L, Sedlarikova L, Hajek R, Sevcikova S (2012) TGF-beta-an excellent servant but a bad master. *J. Transl. Med.* **10**, 183.

20 Lutty G, Ikeda K, Chandler C, McLeod DS (1991) Immunohistochemical localization of transforming growth factor-β in human photoreceptors. *Curr. Eye Res.* **10**, 61–74.

21 Dollery CM, McEwan JR, Henney AM (1995) Matrix metalloproteinases and cardiovascular disease. *Circ. Res.* **77**, 863–868.

22 Verma RP, Hansch C (2007) Matrix metalloproteinases (MMPs): chemical-biological functions and (Q) SARs. *Bioorg. Med. Chem.* **15**, 2223–2268.

23 Bauvois B (2012) New facets of matrix metalloproteinases MMP-2 and MMP-9 as cell surface transducers: outside-in signaling and relationship to tumor progression. *BBA Rev. Cancer* **1825**, 29–36.

24 Jordà M, Olmeda D, Vinyals A, Valero E, Cubillo E, Llorens A *et al.* (2005) Upregulation of MMP-9 in MDCK epithelial cell line in response to expression of the Snail transcription factor. *J. Cell Sci.* **118**, 3371–3385.

25 Umrani RD, Paknikar KM (2014) Zinc oxide nanoparticles show antidiabetic activity in streptozotocin-induced Type 1 and 2 diabetic rats. *Nanomedicine* **9**, 89–104.
26 Dutta RK, Nenavathu BP, Gangishetty MK, Reddy AVR (2013) Antibacterial effect of chronic exposure of low concentration ZnO nanoparticles on *E. coli*. *J. Environ. Sci. Health A* **48**, 871–878.
27 Guo D, Wu C, Jiang H, Li Q, Wang X, Chen B (2008) Synergistic cytotoxic effect of different sized ZnO nanoparticles and daunorubicin against leukemia cancer cells under UV irradiation. *J. Photochem. Photobiol. B* **93**, 119–126.
28 Kim AR, Ahmed FR, Jung GY, Cho SW, Kim DI, Um SH (2013) Hepatocyte cytotoxicity evaluation with zinc oxide nanoparticles. *J. Biomed. Nanotechnol.* **9**, 926–929.
29 Roy R, Parashar V, Chauhan LKS, Shanker R, Das M, Tripathi A *et al.* (2014) Mechanism of uptake of ZnO nanoparticles and inflammatory responses in macrophages require PI3K mediated MAPKs signaling. *Toxicol. In Vitro* **28**, 457–467.
30 Guo D, Bi H, Wu Q, Wang D, Cui Y (2013) Zinc oxide nanoparticles induce rat retinal ganglion cell damage through bcl-2, caspase-9 and caspase-12 pathways. *J. Nanosci. Nanotechnol.* **13**, 3769–3777.
31 Wang D, Guo D, Bi H, Wu Q, Tian Q, Du Y (2013) Zinc oxide nanoparticles inhibit Ca^{2+}-ATPase expression in human lens epithelial cells under UVB irradiation. *Toxicol. In Vitro* **27**, 2117–2126.
32 Guo D, Bi H, Wang D, Wu Q (2013) Zinc oxide nanoparticles decrease the expression and activity of plasma membrane calcium ATPase, disrupt the intracellular calcium homeostasis in rat retinal ganglion cells. *Int. J. Biochem. Cell B.* **45**, 1849–1859.
33 Wu Q, Guo D, Bi H, Wang D, Du Y (2013) UVB irradiation-induced dysregulation of plasma membrane calcium ATPase1 and intracellular calcium homeostasis in human lens epithelial cells. *Mol. Cell. Biochem.* **382**, 263–272.
34 Lauffenburger DA, Horwitz AF (1996) Cell migration: a physically integrated molecular process. *Cell* **84**, 359–369.
35 Hackenberg S, Scherzed A, Technau A, Froelich K, Hagen R, Kleinsasser N (2013) Functional responses of human adipose tissue-derived mesenchymal stem cells to metal oxide nanoparticles in vitro. *J. Biomed. Nanotechnol.* **9**, 86–95.
36 Zhou EH, Watson C, Pizzo R, Cohen J, Dang Q, de Barros PMF *et al.* (2014) Assessing the impact of engineered nanoparticles on wound healing using a novel in vitro bioassay. *Nanomedicine* **20**, 1–13.
37 Kassen SC, Ramanan V, Montgomery JE, T Burket C, Liu CG, Vihtelic TS *et al.* (2007) Time course analysis of gene expression during light-induced photoreceptor cell death and regeneration in albino zebrafish. *Dev. Neurobiol.* **67**, 1009–1031.
38 Suzuki Y, Tada-Oikawa S, Ichihara G, Yabata M, Izuoka K, Suzuki M *et al.* (2014) Zinc oxide nanoparticles induce migration and adhesion of monocytes to endothelial cells and accelerate foam cell formation. *Toxicol. Appl. Pharm.* **278**, 16–25.
39 Akhtar MJ, Ahamed M, Kumar S, Khan MM, Ahmad J, Alrokayan SA (2012) Zinc oxide nanoparticles selectively induce apoptosis in human cancer cells through reactive oxygen species. *Int. J. Nanomedicine* **7**, 845.
40 Goumans MJ, van Zonneveld AJ, ten Dijke P (2008) Transforming growth factor β-induced endothelial-to-mesenchymal transition: a switch to cardiac fibrosis?. *Trends Cardiovas. Med.* **18**, 293–298.
41 Potenta S, Zeisberg E, Kalluri R (2008) The role of endothelial-to-mesenchymal transition in cancer progression. *Br. J. Cancer* **99**, 1375–1379.
42 Beal MF (1995) Aging, energy, and oxidative stress in neurodegenerative diseases. *Ann. Neurol.* **38**, 357–366.
43 Shimizu H, Hirose Y, Nishijima F, Tsubakihara Y, Miyazaki H (2009) ROS and PDGF-beta receptors are critically involved in indoxyl sulfate actions that promote vascular smooth muscle cell proliferation and migration. *Am. J. Physiol. Cell Physiol.* **297**, C389–C396.
44 Nel A, Xia T, Mädler L, Li N (2006) Toxic potential of materials at the nanolevel. *Science* **311**, 622–627.
45 Kang X, Xie Q, Zhou X, Li F, Huang J, Liu D *et al.* (2012) Effects of hepatitis B virus S protein exposure on sperm membrane integrity and functions. *PLoS One* **7**, e33471.
46 Pan Q, Qiu WY, Huo YN, Yao YF, Lou MF (2011) Low levels of hydrogen peroxide stimulate corneal epithelial cell adhesion, migration, and wound healing. *Invest. Ophthalmol. Vis. Sci.* **52**, 1723–1734.
47 Boulaaba M, Mkadmini K, Tsolmon S, Han J, Smaoui A, Kawada K *et al.* (2013) In vitro antiproliferative effect of arthrocnemum indicum extracts on Caco-2 cancer cells through cell cycle control and related phenol LC-TOF-MS identification. *Evid. Based Complement. Alt. Med.* **2013**, 529375.
48 Ahmad J, Alhadlaq HA, Siddiqui MA, Saquib Q, Al-Khedhairy AA, Musarrat J *et al.* (2013) Concentration-dependent induction of reactive oxygen species, cell cycle arrest and apoptosis in human liver cells after nickel nanoparticles exposure. *Environ. Toxicol.* 2013 Jun 17. doi: 10.1002/tox.21879. [Epub ahead of print].
49 Massague J, Blain SW, Lo RS (2000) Reviews-TGFb signaling in growth control, cancer, and heritable disorders. *Cell* **103**, 295–310.
50 Peschon JJ, Slack JL, Reddy P, Stocking KL, Sunnarborg SW, Lee DC *et al.* (1998) An essential role for ectodomain shedding in mammalian development. *Science* **282**, 1281–1284.